Some factors affecting retrogressive failure of sensitive clay slopes using large deformation finite element modeling

GEOQuébec 2015
Challenges from North to South
Des défis du Nord au Sud

Chen Wang, Biswajit Saha and Bipul Hawlader
Memorial University of Newfoundland, St. John's, Canada

ABSTRACT
Many landslides in sensitive clay slopes near the riverbank in Eastern Canada and Scandinavia have been reported in the literature. Some of them extended over a large horizontal distance from the river bank. Traditional limit equilibrium methods cannot explain such failure because the failure surfaces develop progressively. Finite element (FE) modeling of such failure is also very challenging because significant strain localization occurs along the failure plane (shear band) that results in unacceptable mesh distortion. Moreover, the failed soil mass might displace a very large distance. The process of failure of sensitive clay slopes due to toe erosion is simulated using a large deformation FE modeling technique. Post-peak degradation of undrained shear strength and its effects on progressive failure surface development are examined. The effects of some factors, such as the amount of toe erosion, initial stress conditions (K_0) and height of the slope, are investigated. It is shown that these factors could change the failure patterns of sensitive clay slopes near the river bank.

RÉSUMÉ
De nombreux glissements de terrain survenus dans des zones d'argiles sensibles situées à proximité de rives de cours d'eau dans l'Est du Canada et la Scandinavie ont été rapportés dans la littérature. Certains d'entre eux s'étendent sur une grande distance horizontale à partir de la berge. Les méthodes traditionnelles d'équilibre limite ne peuvent pas expliquer de telles ruptures, parce que leurs surfaces se développent progressivement. La modélisation par éléments finis (EF) de ce type de rupture est également très difficile, parce que des zones de déformations importantes se produisent le long du plan de rupture (bande de cisaillement) ce qui entraîne une distorsion inacceptable du maillage. En outre, la masse de sol en rupture se déplace sur une distance importante. Le processus de rupture des pentes dans des argiles sensibles amorcé par de l'érosion en pied de talus est modélisé à l'aide d'une technique de modélisation EF permettant de grandes déformations. La dégradation post-pic de la résistance au cisaillement non drainée et ses effets sur le développement progressif de la surface de rupture sont examinés. Les effets de certains facteurs, comme l'importance de l'érosion en pied de talus, les conditions de contraintes initiales (K0), ainsi que l'importance de la pente sont examinés. Il est démontré que ces facteurs peuvent changer les modes de rupture en zones d'argiles sensibles situées à proximité des berges de cours d'eau.

1 INTRODUCTION

Many landslides in sensitive clays near the river bank in Eastern Canada and Scandinavia have been reported in the literature. Most of these large-scale landslides are progressive in nature. Analyzing failure patterns, Locat et al. (2011) categorized retrogressive landslides in sensitive clays into three groups: (a) flow, (b) translational progressive landslide, and (c) spread. Upward progressive failure might be initiated due to excavation, erosion or small slides in the river bank slopes (Quinn et al., 2007; Locat et al., 2008; Demers et al., 2013). Although the limit equilibrium method has been widely used for slope stability analysis, these large-scale landslides cannot be explained using the limit equilibrium methods because the failure surfaces develop progressively due to strain-softening of sensitive clay. Conceptual models have been proposed in the past to explain the possible mechanisms involved in failure (Odenstad, 1951; Carson, 1977; Carson, 1979). Using the concepts of linear elastic fracture mechanics, Quinn et al. (2011) proposed an analytical model to calculate the development of shear band in a simplified slope with a vertical cut. Attempts have been also taken in the past to model this behaviour using finite element (FE) modeling techniques (Locat et al., 2013, 2015). However, FE modeling in Lagrangian framework suffers from numerical issues related to unacceptable mesh distortion and lack of convergence because significant strain localization occurs in the failure planes develop through sensitive clays. Therefore, the FE analyses in previous studies have been performed for some idealized conditions.

In a recent study, Dey et al. (2015a) used an advanced numerical modeling technique to simulate the failure of sensitive clay slopes. The analyses have been conducted using Abaqus CEL, in which soil flow through the fixed mesh and therefore mesh distortion is not expected. They successfully simulated the formation of horst and graben in spread type of failure. A critical review of existing FE modeling techniques and advantages of Abaqus CEL for modeling sensitive clay slope have been presented elsewhere (Dey et al., 2014, 2015a,b) and are not repeated here.

The aim of the present study is to examine numerically the conditions responsible for different failure patterns as observed in the field. To this end, three factors are considered in this study: (i) amount of toe erosion, (ii) in-situ effective stress and (iii) height of the slope. All the analyses are performed for the failure of the slope in undrained condition.

2 PROBLEM DEFINITION

An idealized sensitive clay slope near the riverbank analyzed in this study is shown in Fig. 1. The slope has three layers of soil: a crust of overconsolidated clay near the ground surface and face of the slope, a sensitive clay layer beneath the crust, and a stiff base layer at the bottom of the slope. The thicknesses of the soil layers are denoted as H_c, H_s and H_b, as shown in Fig. 1. The slope of the river bank (β) equal to 30°. Erosion and/or excavation near the toe of the slope is considered as the triggering factor of slope failure. The height of the erosion/excavation is H_e. In order to simulate the erosion, a soil block referred as "erosion block" is set at the toe of the slope (hatched zone in Fig. 1). The erosion block is moved leftward horizontally (displacement is referred as Δ) during the simulation. For simplicity, the water table is assumed at the ground surface and river is full. Analyses are performed for undrained condition because the failure of the slope may occur in a very short period of time (Locat et al., 2013).

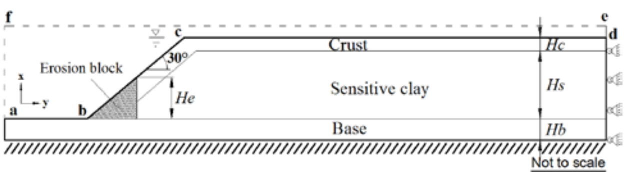

Figure 1. Geometry of the slope used in FE modeling

The effects of the following factors on stability and failure patterns of the slope are analyzed: (i) the size of the erosion/excavation block, (ii) at-rest earth pressure coefficient K_0, and (iii) slope height (H_s+H_c). FE analyses are conducted for the following three cases. Further details of the geometry and some soil parameters used in these analyses are shown in Table 1.

Case-1: The aim of these analyses is to show the effects of toe erosion/excavation on stability of the slope. FE analyses are performed for 5 m and 10 m erosion/excavation block at the toe (i.e. H_e=5 and 10 m in Fig. 1) and the slope height is 19 m. The at-rest earth pressure coefficient K_0=1 is used.

Case-2: In order to check the effects of earth pressure coefficient K_0, FE simulations are performed for K_0=0.7, 0.9, 0.93 and 0.95. The geometry of the slope in this case is same as in Case-1.

Case-3: The effects of slope height (H_s+H_c in Fig. 1) on the failure pattern are investigated from this analysis. In this case, the height of the slope is 22 m, which is 3 m higher than the slope analyzed in Case-1.

Table 1. Geometry and K_0 for different cases

Case #	H_e (m)	H_c (m)	H_s (m)	H_b (m)	K_0
1	5&10	3	16	5	1.0
2	10	3	16	5	0.70,0.90,0.93&0.95
3	10	3	19	5	1.0

3 FINITE ELEMENT MODELING

Abaqus 6.12 FE software is used in this study for numerical analysis. The retrogressive failure simulated in this study is fundamentally a large deformation problem. Conventional FE modeling techniques developed in Lagrangian framework cannot model such large deformation problems properly because significant mesh distortion occurs. In order to overcome these issues, the Coupled Eulerian-Lagrangian (CEL) technique currently available in Abaqus FE software is used. The performance of Abaqus CEL in modeling sensitive clay slopes have been discussed in previous studies (Dey et al. 2014, 2015a,b). In Abaqus CEL, the Eulerian material (soil) can flow through the fixed mesh. Therefore, there is no numerical issue of mesh distortion or mesh tangling even at large strains in the zone around the failure plane.

The FE model consists of three parts: (i) soil, (ii) the erosion block and (iii) void space (i.e. space abcdefa in Fig. 1) to accommodate the displaced soil mass. The soil is modeled as Eulerian material using EC3D8R elements, which are 8-noded linear brick elements. The erosion block is modeled in Lagrangian framework as a rigid body, which makes the model computationally efficient. Soil and void spaces are created in Eulerian domain using Eulerian Volume Fraction (EVF) tool. For void space EVF is zero (i.e. no soil). On the other hand, EVF is unity inside the slope geometry, which means these elements are filled with Eulerian materials of three different types of soil.

Only three-dimensional model can be generated in Abaqus CEL. In the present study, the model is only one element thick in the out of plane direction. The movement of soil perpendicular to the *x-y* plane in Fig. 1 is restricted by applying zero velocity boundary condition in order to mimic plane strain condition. On the bottom of the model all velocity components are zero. In addition, zero velocity boundary condition is applied at the right side of the model. The failed soil might move leftward a very long distance. Hence, a free boundary is set at the left side of the Eulerian domain such that the soil can move out of the domain from the left boundary such that there is no accumulation of soil behind this boundary.

The numerical analysis mainly consists of two steps of loading. In the first step geostatic load is applied to bring the soil in in-situ condition. A FORTRAN subroutine is used to set the earth pressure coefficient K_0. In the second step, the erosion block is displaced leftward to simulate erosion/excavation at the toe.

4 UNDRAINED SHEAR STRENGTH OF SOIL

Laboratory tests (e.g. Tavenas et al., 1983; Bjerrum and Landva, 1966; Bernander, 2000) show that the undrained shear strength of sensitive clay decreases with plastic shear strain. The post-peak softening behavior of sensitive clay is implemented in the present FE modeling. The shear strain could be localized in a very small zone along the shear band. The thickness of shear band is very difficult to estimate in laboratory experiments or in the field. Hence, shear displacement is used to define the post-peak softening curve while the shear strain is used in the pre-peak elastic region, which has been also recommended by other researchers (e.g. Quinn et al., 2011).

Linear variation of s_u with plastic shear displacement has been used by some previous researchers for modeling strain-softening behavior of sensitive clays (e.g. Quinn et al., 2011, 2012; Locat et al., 2013, 2015). However, the following exponential relationship of shear strength degradation, as a function of plastic shear displacement, better represents the post-peak softening behaviour as observed in laboratory tests (Dey et al., 2012, 2013, 2015).

$$s_u = [1+(S_t-1)\exp(-3\delta/\delta_{95})]s_{uR} \quad [1]$$

where, s_u is the mobilized undrained shear strength at displacement δ; S_t is the sensitivity of the soil; $\delta = \delta_{total} - \delta_p$ where δ_p is the displacement required to attain the peak undrained shear strength (s_{up}); and δ_{95} is the value of δ at which the undrained shear strength of the soil is reduced by 95% of (s_{up}-s_{uR}). Equation [1] is a modified form of strength degradation equation proposed by Einav and Randolph (2005) but in terms of displacement. In this study, Eq. [1] is used to simulate the strain-softening behavior. Fig. 2 shows the relationship between the shear strength and shear displacement. Line oa defines the linear elastic pre-peak behavior. The peak undrained shear strength (s_{up}) is mobilized at point a and remains constant up to point b for a displacement of δ_{pc}. The curve bcd is defined by Eq. 1. After the soil reaches its residual shear strength (s_{uR}), the mobilized shear strength will reduce slowly with shear displacement. The reduction of s_u in this zone is defined by a linear line de, which shows that the shear strength reduces to a small value s_{uld} at large displacement δ_{ld}. The shear strength after this displacement remains constant at s_{uld}.

Adopting the von-Mises yield criterion, the degradation of undrained shear strength of sensitive clay is given as an input in the FE model by varying yield strength ($=2s_u$) as a function of plastic shear strain (γ_p), in which γ_p is calculated as $\gamma_p=\delta/t$ assuming simple shear condition, where t is the thickness of the shear band. In this study, $t=t_{FE}$ is used, where t_{FE} is the thickness of the cubical EC3D8R finite element. The soil parameters of the crust and sensitive clay used in FE modeling are shown in Table 1. The base layer is assumed to be very stiff and simulated as elastic material with Young's modulus E=200 MPa.

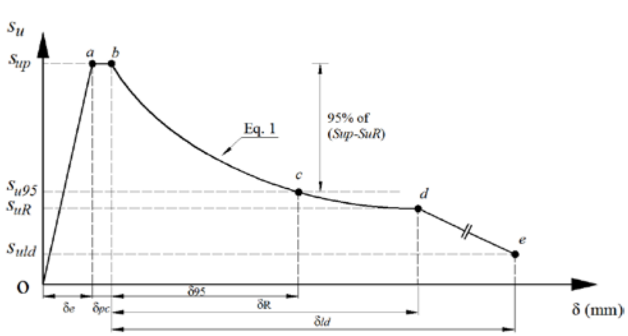

Figure 2. Stress–displacement behaviour of sensitive clay

Table 2. Soil parameters used in FE modeling

Crust	
Undrained Young's modulus, E_u (MPa)	10
Poisson's ratio, ν_u	0.495
Undrained shear strength, s_u (kPa)	50
Submerged unit weight of soil, γ' (kN/m^3)	9.0
Sensitive clay	
Undrained Young's modulus, E_u (MPa)	7.5
Poisson's ratio, ν_u	0.495
Peak undrained shear strength, s_{up} (kPa)	37.5
Residual shear strength, s_{uR} (kPa)	7.5
Large displacement undrained shear strength, s_{uld} (kPa)	2.0
Submerged unit weight of soil, γ' (kN/m^3)	8.0
Plastic shear displacement for 95% degradation of soil strength, δ_{95} (mm)	30
Plastic shear displacement for initiation of softening, δ_{pc} (mm)	4
Plastic shear displacement for large displacement undrained shear strength, δ_{ld} (mm)	2000

5 FINITE ELEMENT RESULTS

Strain concentration and formation of shear band is examined using the equivalent plastic strain (PEEQVAVG), which represents the integration of plastic deviatoric strain rate tensor over the period of analysis. If PEEQVAVG>0 plastic strains generate.

5.1 Effects of Toe Erosion

Fig. 3 shows the simulation results of a 19 m height of slope for displacement of a 5.0 m erosion block. As shown in Fig. 3(a), after the geostatic step, no plastic strain develops in the slope. Analysis has been also carried out for the same slope replacing the erosion block with soil having geotechnical properties of the crust. No plastic strain in the soil has been found, which indicates that the slope is stable for the in-situ state of stress condition before toe erosion. In the following step, the erosion block is moved leftward gradually, which increases shear stress in the soil. When shear displacement of an element exceeds $\delta_e+\delta_{pc}$ (Fig. 2), degradation of s_u occurs resulting in formation of a shear band. In this case, a shear band propagates horizontally as shown in Figs. 3(b) and 3(c). The erosion block separates from the remaining soil when it is moved 0.55 m to the left. At that time a horizontal shear band of 106 m length is formed. As expected, further displacement of the erosion block does not have any change in stresses or strains in the slope or shear band.

Fig. 3(d) shows the Mises stress in the soil when the erosion block is displaced to distance more than 0.55 m. Large shear stress generates in the soil elements near the point A. The Mises stress in some elements increases almost to the yield strength of the soil ($2s_u$), which indicates that a failure plane is expected to be formed at this location.

Although a long horizontal shear band forms, global failure of the slope does not occur in this case. However, this slope would be prone to failure due to additional triggering factors, such as construction in the upslope areas, because the shear strength along the horizontal shear band reduces significantly.

(a) Δ=0.00 m

(b) Δ=0.05 m

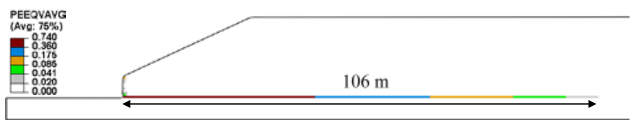

(c) Δ≥0.55 m

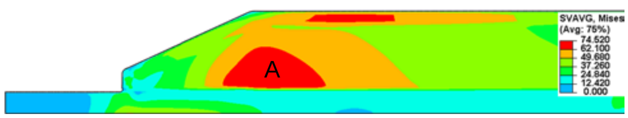

(d) Δ≥0.55 m

Figure 3. Formation of shear band in Case-1 for 5 m toe erosion

Analysis is also performed for the same slope as above but for a 10 m toe erosion. Fig. 4 shows the development of shear band with displacement of erosion block. Fig. 4(a) shows that when the erosion block is displaced to 0.7 m a horizontal shear band of 110 m forms. After that a curved failure plane develops when the erosion block is displaced to 0.65 m. With further displacement, another shear band develops from the curved failure plane and propagates downward to the previously formed horizontal shear band and forms a "horst" (Fig. 4c). As shown in Fig. 4(d), upward propagation of another shear band from the horizontal shear band forms a "graben" with increase in Δ. The process continues and a series of horsts and grabens forms above the basal horizontal shear band as shown in Figs. 4(e) and 4(f). Further discussion on formation of horsts and grabens and modeling of spread using Abaqus CEL is available in Dey et al. (2015a).

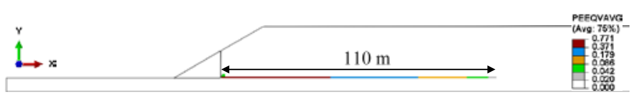

(a) Δ=0.70 m

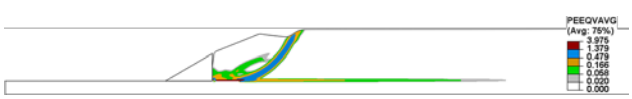

(b) Δ=2.65 m

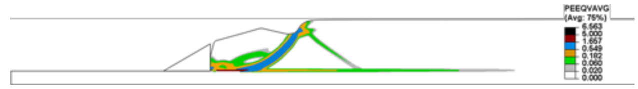

(c) Δ=4.88 m

(d) Δ=16.20 m

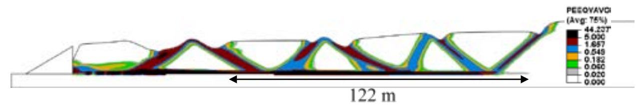

(e) Δ=57.76 m

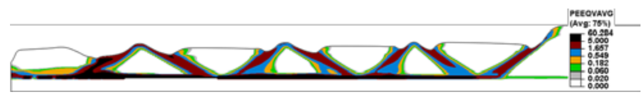

(f) Δ>80.00 m

Figure 4. Spread in Case-1 for 10 m toe erosion

The following conclusions can be drawn from these two analyses:

- Small amount of erosion or landslide at the toe can generate a horizontal shear band through the sensitive clay without global failure. The slope might be globally stable; however, because of significant strength reduction in the shear band, the potential of failure of this slope due to additional triggering factors is high.
- With increase in size of the erosion block, retrogressive failure occurs which is successfully simulated using the present FE modeling technique.

5.2 Effects of Earth Pressure Coefficient at Rest (K_0)

Fig. 5 shows the simulation of a 19 m slope which is same as the simulation presented in Fig. 4 except for the earth pressure coefficient K_0 =0.70 (i.e. K_0 =1.0 in Fig. 4). As shown in Fig. 5(a), after geostatic step, the Mises stress increases with depth because $K_0 \neq 1.0$ in this case. As shown in Figs. 5(b) and 5(c), with displacement of the erosion block, a shear band develops from the toe. However, different from Case-1, the shear band does not propagate horizontally but a curved failure surface develops resulting in a rotational slide. Figs. 5(d) and 5(e) show the instantaneous velocity vectors, which indicate that the failed soil mass displaces along the slide surface. When the failed soil mass moves sufficiently large distance, the lateral support to the soil behind the scrap is reduced. However, this reduction is not sufficient to cause the formation of another failure plane as in Fig. 4.

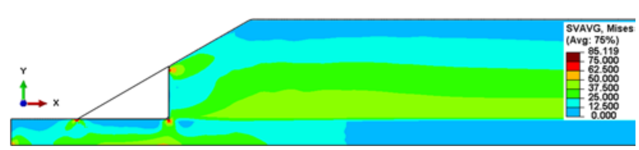

(a) Δ=0.00 m

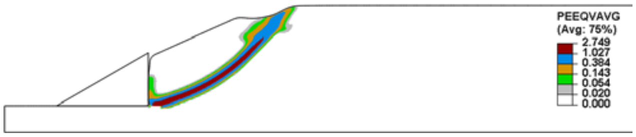

(b) Δ=2.82 m

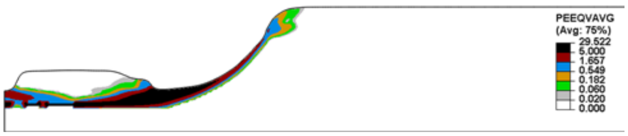

(c) Δ=30.0 m

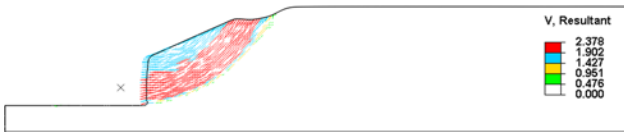

(d) Δ=2.82 m

(e) Δ=30 m

Figure 5. Failure process of the slope with K_0=0.70

As the failure process completely changes from a multiple horsts and grabens (Fig. 4) to a single rotational slide (Fig. 5) due to change in K_0 only, the effects of K_0 is examined further with three more values of K_0.

Fig. 6 shows the failure of the slope with K_0=0.90. Different from the simulation with K_0=0.70 (Fig. 5), the shear band first propagates horizontally when the erosion block is displaced leftward (Fig. 6a). Fig. 6(b) shows that, with displacement of the erosion block, the shear band propagates 20.5 m horizontally and then upward to the ground surface, forming a curved slide surface. The failed soil mass then slides downward with Δ. With further displacement the failed soil mass breaks into several soil blocks as shown in Fig. 6(c).

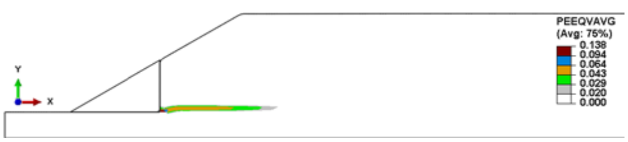

(a) Δ=0.13 m

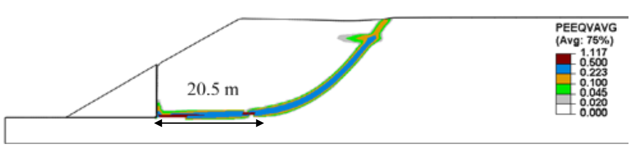

(b) Δ=0.58 m

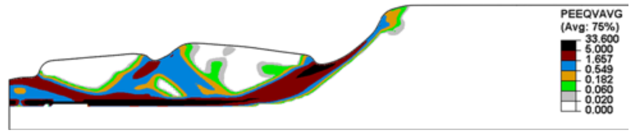

(c) Δ=30.0

Figure 6. Failure process of the slope with K_0=0.90

Simulation with K_0=0.93 is shown in Fig. 7. Comparison of failure patterns in Figs. 6 and 7 shows that for a small change in K_0 from 0.90 to 0.93 the failure pattern changes from single rotational slide to spread. Fig. 7(a) shows that before the first rotational slide, the shear band propagates horizontally 69.5 m which is shorter than in Case-1 (110 m) for K_0=1.0 (Fig. 4a). Then, the first slide occurs near the slope (see Fig. 7b). It is found that the first horst forms when the height difference between the ground surface and the top of the failed soil mass is approximately 9.0 m (Fig. 7c). Compared to Case-1 (Fig. 4c), the failed soil mass displaces further when the first horst forms. Because of lower K_0 value, the reduction of lateral support from the failed soil mass is small in Fig. 7 as compared to Fig. 4. Figs. 7(d) and 7(e) show the formation of subsequent horsts and grabens with displacement of the erosion block.

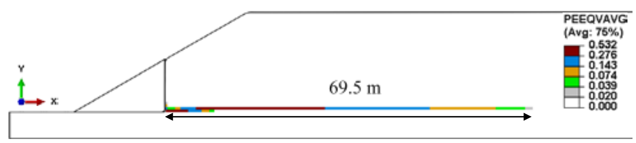

(a) Δ=0.48 m

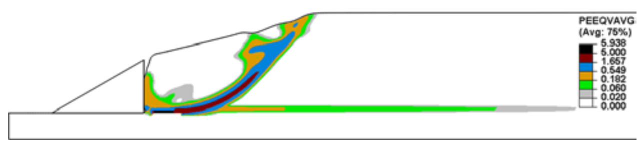

(b) Δ=3.25 m

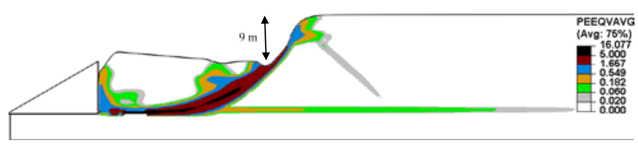

(c) Δ=13.25 m

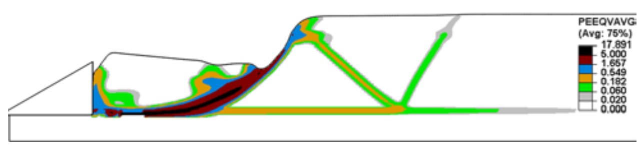

(d) Δ=14.26 m

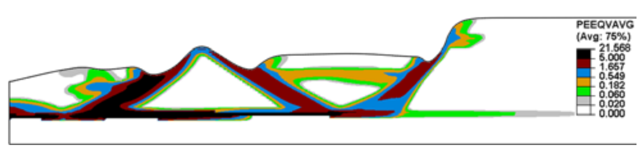

(e) Δ=30.00 m

Figure 7. Failure process of the slope with K_0=0.93

Although it is not shown, the analysis has also been performed for K_0=0.95 and it is found that the propagation of the horizontal shear band is 76 m before the first curved failure surface forms. Therefore, it can be concluded that the propagation of the horizontal shear band increases with K_0. The extent of failure due to toe erosion also increases with the length of the horizontal shear band. In summary, these simulations show that K_0 has a significant influence on failure pattern and extent of failure.

5.3 Effects of Slope Height

In order to check the effects of slope height, an analysis has been performed for a slope of 22 m total height (H_s=19 m H_c=3 m) and a 5 m toe erosion. As in Case 1, K_0=1.0 is used in this simulation. Fig. 8 shows that a 5 m toe erosion is sufficient to trigger retrogressive failure in this case, while retrogressive failure did not occur in Fig. 3 for 19 m slope height. This is because of increase in driving force with slope height. However, the failure pattern shown in Fig. 8 is different from Figs. 4–7. In Fig. 8, initially the shear band propagates horizontally. As the erosion block displaces, a curved shear band forms from the tip of the horizontal shear band and reach the ground surface resulting in a global failure of the slope (Figs. 8b and 8c). With displacement of the erosion block, a number of internal shear surfaces develop in the failed soil mass (Fig. 8c). When the failed soil mass moves a significantly large distance, the lateral support on remaining soil reduces, which causes the formation of another shear band as shown in Fig. 8(d). This process continues until the analysis is stopped (Figs. 8d–8f).

(a) Δ=0.07 m

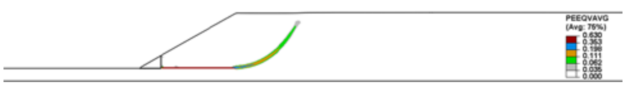

(b) Δ=0.54 m

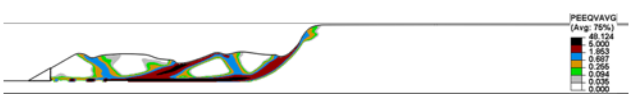

(c) Δ=39.6 m

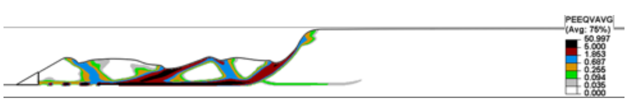

(d) Δ=48.87 m

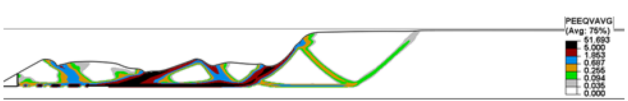

(e) Δ=57.04 m

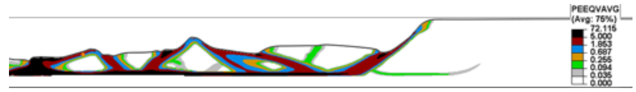

(f) Δ=80.00 m

Figure 8. Failure process of the slope in Case-3

6 CONCLUSIONS

The failure of sensitive clay slopes near the riverbank is simulated using Abaqus CEL. The propagation of shear bands and large displacement of the failed soil mass during the process of retrogressive failure are successfully simulated. Based on the parametric study, the following conclusions can be drawn:

1. A shear band might be formed horizontally due to toe erosion. If the erosion is not large enough, global failure may not occur although a significant reduction of shear strength occurs along the shear band, which should be considered for stability analysis of slope for additional triggering factors.
2. In-situ effective stress condition significantly influences the pattern of failure of the slope due to toe erosion. The length of propagation of the horizontal shear band increases with K_0. When K_0 is close to 1.0, spread failure occurs for the cases analyzed in this study. Moreover, the retrogression distance increases with K_0.
3. The height of the slope may change the pattern of failure. With increasing height, smaller toe erosion may trigger retrogressive failure.

ACKNOWLEDGEMENTS

The works presented in this paper have been supported by the Research and Development Corporation of Newfoundland and Labrador, NSERC and MITACS. The authors express their sincere thanks to Rajib Dey for his valuable suggestions and help with FE modeling.

REFERENCES

Bernander, S. 2000. Progressive failure in long natural slopes: formation, potential extension and configuration of finished slides in strain-softening soils. *Licentiate Thesis*, Luleå University of Technology.

Bjerrum, L. and Landva, A. 1966. Direct simple-shear tests on a Norwegian quick clay. *Géotechnique*, 16(1): 1-20.

Carson, M. A. 1977. On the retrogression of landslides in sensitive muddy sediments. *Canadian Geotechnical Journal*, 14(4): 582-602.

Carson, M. A. 1979. On the retrogression of landslides in sensitive muddy sediments: Reply. *Canadian Geotechnical Journal*, 16(2): 431-444.

Demers, D., Robitaille, D., Locat, P., and Potvin, J. 2013. Inventory of large landslides in sensitive clay in the province of Quebec, Canada: preliminary analysis. *In: Proceedings of the 1st International Workshop on Landslides in Sensitive Clays, Landslides in Sensitive Clays - From Geosciences to Risk Management*, Québec.

Dey, R., Hawlader, B., Phillips, R. and Soga, K. 2012. Effects of shear band propagation on submarine landslide. *In: Proceedings of the 22nd International Offshore and Polar Engineering Conference,* Rhodes, Greece, 766-773.

Dey, R., Hawlader, B., Phillips, R. and Soga, K. 2013. Progressive failure of slopes with sensitive clay layers. *In: Proceedings of the 18th International Conference on Soil Mechanics and Geotechnical Engineering,* Paris, 2177-2180.

Dey, R., Hawlader, B., Phillips, R. and Soga, K. 2014. Stability analysis of a river bank slope with an existing shear band. *6th Canadian GeoHazards Conference*, Kingston, Ontario.

Dey, R., Hawlader, B., Phillips, R. and Soga, K. 2015a. Large deformation finite element modeling of progressive failure leading to spread in sensitive clay slopes. *Géotechnique*. (Accepted).

Dey, R., Hawlader, B., Phillips, R. and Soga, K. 2015b. Modeling of large deformation behaviour of marine sensitive clays and its application to submarine slope stability analysis. (Under review).

Einav, I. and Randolph, M. F. 2005. Combining upper bound and strain path methods for evaluating penetration resistance. *International Journal of Numerical Methods Engineering,* 63(14): 1991-2016.

Locat, A., Leroueil, S., Bernander, S., Demers, D., Locat, J. and Ouehb, L. 2008. Study of a lateral spread failure in an eastern Canada clay deposit in relation with progressive failure: the Saint-Barnabé-Nord slide. *In: Proceedings of the 4th Canadian Conference on Geohazards: From Causes to Management*, Québec, 89–96.

Locat, A., Leroueil, S., Bernander, S., Demers, D., Jostad, H.P. and Ouehb, L. 2011. Progressive failures in eastern Canadian and Scandinavian sensitive clays. *Canadian Geotechnical Journal,* 48(11): 1696-1712.

Locat, A., Jostad, H.P. and Leroueil, S. 2013. Numerical modeling of progressive failure and its implications for spreads in sensitive clays. *Canadian Geotechnical Journal*, 50(9): 961-978.

Locat, A., Leroueil, S., Fortin, A., Demers, D. and Jostad, H. P. 2015. The 1994 landslide at Sainte-Monique, Quebec: geotechnical investigation and application of progressive failure analysis. *Canadian Geotechnical Journal*, 52(4): 490-504.

Quinn, P. E., Diederichs, M. S., Hutchinson, D. J. and Rowe, R. K. 2007. An exploration of the mechanics of retrogressive landslides in sensitive clay. *In: Proceedings of the 60th Canadian Geotechnical Conference*, Ottawa, Ontario, 721-727.

Quinn, P. E., Diederichs, M. S., Rowe, R. K. and Hutchinson, D. J. 2011. A new model for large landslides in sensitive clay using a fracture mechanics approach. *Canadian Geotechnical Journal*, 48(8): 1151-1162.

Quinn, P. E., Diederichs, M. S., Rowe, R. K. and Hutchinson, D. J. 2012. Development of progressive failure in sensitive clay slopes. *Canadian Geotechnical Journal*, 49(7): 782-795.

Odenstad, S. 1951. The landslide at Sköttorp on the Lidan River, February 2, 1946. *Royal Swedish Institute Proceedings*, 4: 1-38.

Tavenas, F., Flon, P., Leroueil, S. and Lebuis, J. 1983. Remolding energy and risk of slide retrogression in sensitive clays. *In: Proceedings of the Symposium on Slopes on Soft Clays,* Linköping, Sweden, SGI Report No. 17, 423-454.